ADVANCED ENERGY MATERIALS

www.advenergymat.de

Sodium–Sulfur Flow Battery for Low-Cost Electrical Storage

*Fengchang Yang, Seyed Mohammad Ali Mousavie, Tae K. Oh, Tairan Yang, Yingqi Lu, Charles Farley, Robert J. Bodnar, Li Niu, Rui Qiao, and Zheng Li**

A new sodium–sulfur (Na–S) flow battery utilizing molten sodium metal and flowable sulfur-based suspension as electrodes is demonstrated and analyzed for the first time. Unlike the conventional flow battery and the high-temperature Na–S battery, the proposed flow battery system decouples the energy and power thermal management by operating at different temperatures for the storage tank (near room temperature) and the power stack (100–150 °C). The new Na–S flow battery offers several advantages such as easy preparation and integration of the electrode, low energy efficiency loss due to temperature maintenance, great tolerance of the volume change of the metal anode, and efficient utilization of sulfur. The Na–S flow battery has an estimated system cost in the range of $50–100 kWh^{-1} which is very competitive for grid-scale energy storage applications.

Among energy storage technologies needed for massive deployment of inherently intermittent renewable energy generation, rechargeable batteries are technically viable solutions to provide most grid energy storage services and have desired features such as emission-free operation, high round-trip efficiency, and low maintenance expense.[1] In particular, lithium-ion batteries, flow batteries, and high-temperature Na–S batteries are three of the most promising grid-scale battery technologies which have been under intensive development for decades.[2] In conventional flow batteries, aqueous redox active solutions are stored in external tanks and pumped through an ion-exchange and electron-extraction power stack to store or deliver electricity. The system power is determined by the size of the stack where the redox reactions happen and the energy of the system is proportional to the size of the tank. The decoupled system energy and power makes the battery easy to scale up. However, the energy density of the aqueous solution is limited by the solubility of the redox species (e.g., 1–2 M for vanadium redox flow battery, VRFB) and the electrochemical window of water (≈1.5 V), which leads to relatively low energy density and contributes to their high system cost.[2b,c] Promising new approaches to increase the energy density of the reactants include semi-solid flow batteries (SSFBs) using suspensions of solid storage compounds as flow electrodes,[3] and several new classes of solution reactants including lithium polysulfide solutions,[4] all-organic redox couples,[5] and ionic liquid-based complexes.[6] Among these new approaches, SSFBs have the potential to overcome both limitations of aqueous solution energy density.[3d,7] Semi-solid suspension is composed of nanoscale carbon forming continuous conductive network and densely packed larger solid storage materials particles suspended in electrolytes. SSFB approach can significantly increase the system energy density by storing energy in solid phase instead of liquid phase that increases nominal molar concentration of redox active species and expanding electrochemical window when nonaqueous solvent is used in the electrolyte. Another aforementioned promising battery technology for grid storage, high temperature Na–S battery, has many appealing features such as low-cost raw materials, high theoretical specific energy, high energy efficiency, and good cycle life.[8] Traditionally, these batteries operate at high temperatures (300–350 °C). In addition to incurring significant cost in thermal management, many other safety and reliability issues arise from the high operating temperature, e.g., the corrosion of current collectors and battery casing, the degradation of solid electrolyte membrane (typically made of β''-Al_2O_3, abbreviated as BASE), and potential for explosion when the membrane is damaged. To resolve these issues, a number of groups have studied room-temperature Na–S batteries using polymeric membranes and organic electrolytes. While exciting progresses have been made, these batteries often suffer from problems such as chemical self-discharging due to the shuttling mechanism, formation of metallic sodium dendrites, and the poor utilization of the sulfur cathodes.[9] An alternative strategy of mitigating the issues of high-temperature and room-temperature Na–S batteries is to operate the battery at intermediate temperature. While this concept was first introduced in the 1980,[10] it received significant attention only quite recently due

Dr. F. Yang,[+] S. M. A. Mousavie, T. K. Oh, T. Yang, Y. Lu, Prof. R. Qiao, Prof. Z. Li
Department of Mechanical Engineering
Virginia Tech
Blacksburg, VA 24061, USA
E-mail: zhengli@vt.edu
Dr. C. Farley, Prof. R. J. Bodnar
Department of Geosciences
Virginia Tech
Blacksburg, VA 24061, USA
Prof. L. Niu
Center for Advanced Research on Analytical Science
Guangzhou University
Guangzhou 510006, P. R. China
The ORCID identification number(s) for the author(s) of this article can be found under https://doi.org/10.1002/aenm.201701991.
[+]Dr. F. Yang is currently with JENSEN HUGHES, Inc.

DOI: 10.1002/aenm.201701991

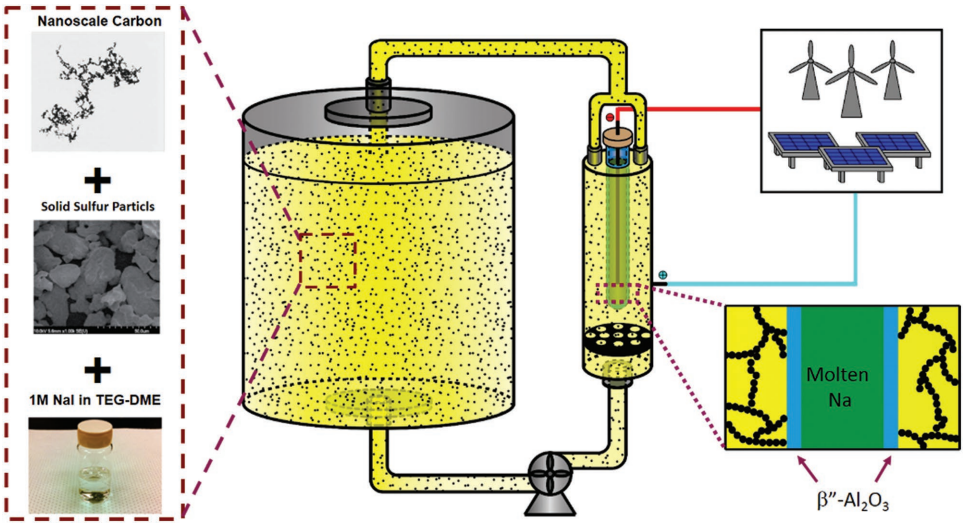

Figure 1. A schematic of the semi-solid Na-S flow battery. Nanoscale carbon picture is reproduced with permission.[3a] Copyright 2011, Wiley-VCH. Solid sulfur particles picture is reproduced with permission.[1e] Copyright 2015, Royal Society of Chemistry.

to the growing demand for grid energy storage.[9b,11] Lu and colleagues demonstrated Na–S battery working at ≈150 °C using BASE as solid electrolyte membrane and tetraglyme as cathode sulfur suspension solvent.[9b] Because the sodium anode is at the molten state above 98 °C, sodium metal dendrites formation is eliminated. The shuttling of polysulfides is also suppressed by the solid electrolyte separator. It has been shown that the rate capacity and cycling stability of these Na–S batteries are improved greatly over those operating at room temperature.[9b] Inspired by the semi-solid approach and sodium polysulfide chemistry at intermediate temperature, we propose a new Na–S flow battery utilizing molten sodium metal and flowable sulfur-based suspension as electrodes. Unlike the conventional flow battery and the high-temperature Na–S battery, the proposed flow battery system decouples the energy and power thermal management by operating at different temperatures for the storage tank (near room temperature) and the power stack (100–150 °C). The Na–S flow battery has an estimated system cost in the range of \$50–100 kWh^{-1} which is very competitive for grid-scale energy storage applications.

Figure 1 shows a schematic of the proposed semi-solid Na–S flow battery. The battery has four main components: a flowable semi-solid sulfur suspension as catholyte, an external storage tank for the suspension, a solution pump, and a current-extracting stack housing a BASE tube filled with molten sodium anode. In the semi-solid suspension, nanoscale carbon and solid sulfur particles are dispersed in 1 M NaI tetraglyme solution. In the power stack, a BASE tube is hosted in a stainless steel (SS) metal casing to serve as the separator which is filled with molten sodium. The semi-solid suspension is stored in the tank at room temperature and pumped into the space between the BASE tube and the casing wall which is maintained at 100–150 °C to keep the sodium at the molten state. During discharging operation, the suspension in the storage tank is pumped intermittently into the stack and is discharged while it is not flowing. During recharging, the discharged suspension in the tank is pumped back into the stack and is charged to store energy.

The proposed semi-solid Na–S flow battery inherits a number of advantages of flow batteries (e.g., excellent scalability of storage capacity due to the decoupling between energy storage and power delivery) and intermediate Na–S batteries (e.g., reduced safety concern due to elimination of the metal dendrite formation and low materials cost associated with earth-abundant sodium and sulfur as active materials). Figure S2 in the Supporting Information compares the theoretical energy density of the Na–S flow battery with the VRFB and the Li-ion battery. It shows that, with a sulfur concentration above ≈1.5 M, the proposed flow battery already offers higher theoretical energy density of the conventional VRFB. By further increasing the sulfur concentration in the suspension (>15 M), our flow battery can potentially compete with Li-ion in term of energy density. In addition, the proposed Na–S flow battery leads to several other advantages over the existing high temperature Na–S and flow batteries. First, it greatly simplifies the preparation of the cathode, which helps reduce the battery manufacturing cost. The flowable semi-solid sulfur suspension can be prepared by simply mixing sulfur and carbon particles and then suspend in Na-ion conducting electrolyte (e.g., 1 M NaI tetraglyme solution). This is different from the existing high or intermediate temperature Na–S battery where the elemental sulfur or polysulfide must be premelted or predissolved and then infused into carbon fiber current collectors to ensure high sulfur utilization rate.[9b] Second, in the present scheme, only the stack has to be kept at intermediate temperature (i.e., 100–150 °C) and the suspension in the storage tank can be left at room temperature. This can minimize the thermal management needed for battery operation and consequently lowers the cost associated with it. Finally, the issues associated with the volume change of electrodes are effectively eliminated. In room temperature Na–S batteries, the large volume change of the sodium anode and sulfur cathode often causes severe cell life and safety problems.[9a,b] Therefore, the sulfur content in the cathode is often intentionally lowered to accommodate such volume change which significantly reduces the practical energy density at the cell level. In our scheme shown in Figure 1, however, the

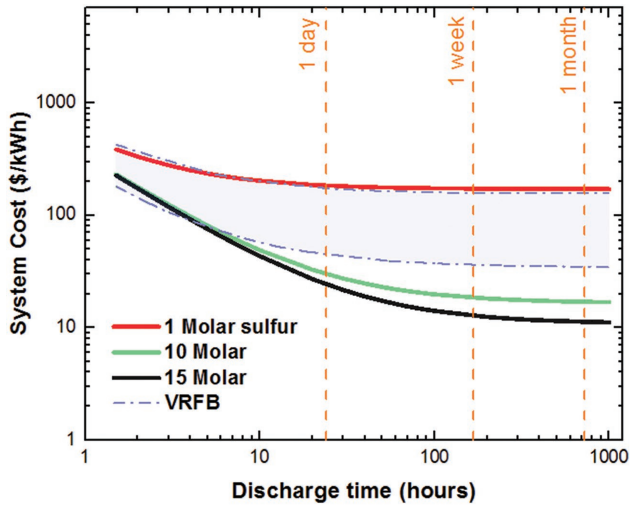

Figure 2. System cost for Na–S semi-solid flow battery with catholyte sulfur nominal concentration of 1, 10, and 15 M.

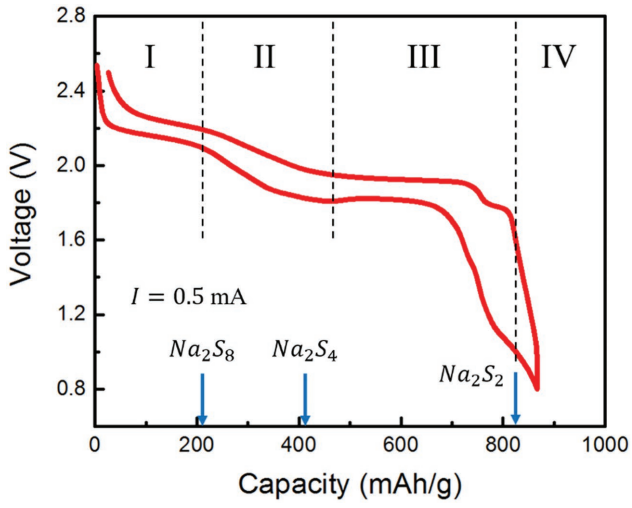

Figure 3. Initial discharge and charge profile of a semi-solid Na–S battery at 150 °C at a constant current of 0.5 mA where the suspension covered membrane area is around 1.2 cm^2 (current density is 0.42 mA cm^{-2}). The blue arrows indicate the theoretical capacities for different polysulfides as the final discharge product. The sulfur suspension catholyte is composed of 1 M sulfur and 1 vol% Ketjen in 1 M NaI TEGDME solution.

height of the molten sodium in the BASE tube is self-adjustable. At the catholyte side, the sulfur and carbon nanoparticles are dispersed in liquid solvents and thus their volume change during charging/discharging is easily accommodated.

Based on the technoeconomic model for flow batteries developed by Darling et al.,[12] the system cost of the proposed Na–S flow battery is estimated and compared with conventional VRFB (**Figure 2** and the Supporting Information for cost model details). Three real curves represent suspension electrodes with 1, 10, and 15 M sulfur nominal concentration and the region between two dashed curves indicate the range of system cost for commercialized VRFB taken from the paper by Darling et al.[12] For 1 M sulfur case, the system cost of Na–S flow battery is similar to the higher cost boundary of the VRFB. As the sulfur nominal concentration increases, the system cost of the proposed Na–S flow battery becomes competitive or even lower than that of the VRFB especially for longer storage duration hours (>10 h) which is the future trend for the development of grid storage batteries based on the emerging use-case studies.

To evaluate the performance of the semi-solid Na–S battery, we first tested the discharging and charging of this battery with 1 M sulfur nominal concentration under nonflow conditions at 150 °C (see **Figure 3**). Since the nominal concentration of elemental sulfur is below the solubility of sulfur in tetraglyme (2.3 M),[9b] the sulfur should exist in the dissolved state as S_8 at the beginning of the discharge. The first discharge capacity of the cell was found to be 864 mA h g^{-1}, which represents the capacity of per gram of sulfur initially in the cathode (including both the soluble and insoluble forms). This capacity is not only higher than that of the intermediate temperature Na–S batteries reported previously (e.g., 473 mA h g^{-1} was reported by Lu et al.),[9b] but also slightly higher than the theoretical capacity of the cell when Na_2S_2 is taken as the final discharge product (836 mA h g^{-1}). The high discharge capacity indicates that sulfur is utilized efficiently in the semi-solid Na–S cell. Two factors contribute to the higher capacity of the proposed Na–S cell than prior cells. First, in the present cell, elemental sulfur is used directly to prepare the cathode. This is different from prior Na–S cells, where the cathodes typically contain a mixture of elemental sulfur and polysulfide at the beginning of discharging and thus part of the sulfur capacity is sacrificed.[9b,10] Second, the discharge proceeds further in the semi-solid suspension cathodes than in previous Na–S cells. Since the measured capacity is higher than the theoretical capacity corresponding to Na_2S_2 as the final discharge product, Na_2S are likely part of the final discharge product. This seems to be consistent with the observations in previous studies of Li–S batteries, where it was observed that using semi-solid suspensions as cathode often allows the discharge to proceed deep into the precipitation regimes that are difficult to reach in other types of cathodes.[3d] Similar to the room-temperature Na–S batteries,[9c,13] the voltage profile can be divided into four regions (I–IV). Region I starts from the beginning of discharge and ends at a capacity of ≈200 mA h g^{-1}. This region features a sharp drop of the cell voltage at the beginning of discharging and a subsequent weak plateau between 2.2 and 2.1 V. Similar weak plateau has been observed in room-temperature Na–S and Li–S batteries and is often attributed to the reaction $S_8 + 2e \rightarrow S_8^{2-}$.[13,14] Associating the weak plateau to this reaction is also partly supported by the observation that the capacity at the end of region I is quite close to the theoretical capacity of Na_2S_8 as the discharge product (209 mA h g^{-1}). Region II starts from ≈200 mA h g^{-1} and ends ≈450 mA h g^{-1}. In this slope region, the voltage decreases from 2.1 to 1.82 V. This region can be attributed to the gradual degradation of S_8^{2-} to S_n^{2-} ($4 \le n < 8$).[9b,13] Here, the discharge voltage is affected by the electrochemical reactions for the formation of lower order polysulfides (e.g., S_5^{2-} and S_4^{2-}), the chemical equilibrium between these polysulfides, and reactions of the polysulfides with Na^+ ions. Because of the low nominal concentration of elemental sulfur in the suspension, the reaction products are mostly soluble (e.g., the solubility of Na_2S_4 is 0.76 M elemental sulfur in tetraglyme, which is only modestly smaller than the 1 M nominal concentration

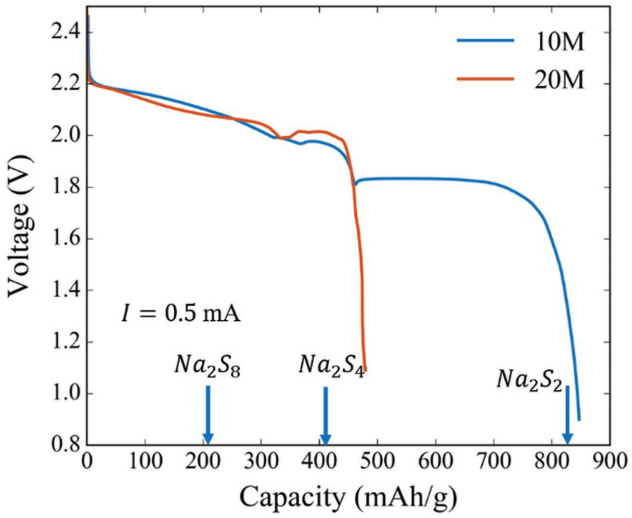

Figure 4. The initial discharging profiles of semi-solid Na–S cells with different sulfur nominal concentration in the cathode suspension. The blue arrows indicate the theoretical capacities for different polysulfides as the final discharge product. The sulfur suspension catholyte contains 2 vol% Ketjen and the electrolyte is 1 M NaI TEGDME solution. The suspension covered membrane area is around 1.2 cm^2.

of sulfur in the suspension), the concentration of polysulfides in the suspension changes smoothly. Consequently, the voltage drops gradually as the discharging proceeds. Previous in situ Raman spectroscopy studies indicated that the reaction product for discharging with voltage characteristics shown here is dominated by Na_2S_4.[11a] This conclusion is also supported by the fact that the storage capacity achieved at the end of region II is close to the theoretical capacity corresponding Na_2S_4 as discharging product (418 mA h g^{-1}). As discharging proceeds beyond region II, a plateau at 1.82 V appears first and this is followed by a sudden drop of the cell voltage toward 1.2 V. The plateau voltage closely resembles that reported in prior studies of intermediate and room temperature Na–S batteries.[9b,13a] Based on the XRD analysis and Raman spectroscopy performed in those studies, the dominant electrochemical reaction in this region is the formation of Na_2S_2 through reduction of high order polysulfides such as $S_4^{2-} + 2e \rightarrow 2S_2^{2-}$. This is consistent with the fact that the reaction products such as Na_2S_2 have low solubility. Specifically, previous simulation studies showed that once metal polysulfide species (e.g., Li_2S_2) in metal–sulfur cells exceeds their solubility, they precipitate out of the solution and the equilibrium between dissolved and precipitated polysulfides helps maintain a nearly constant voltage.[14,15] At the end of the voltage plateau, a sharp drop of voltage toward 1.2 V appears. This voltage drop is likely caused by the solid–solid reaction between Na_2S_2 and Na_2S[13a] or the passivation of the active surface area by the Na_2S_n ($n \leq 2$) precipitating out of the solution.[9b] The last discharge region (region IV) shows a further drop of the cell voltage to ≈0.8 V. Because the total capacity of the discharge process exceeds the theoretical capacity corresponding to Na_2S_2 as the final product (836 mA h g^{-1}), reduction of Na_2S_2 to Na_2S is implicated. The rapid drop of the voltage should have similar origins compared to the last part of Region III because Na_2S also has very low solubility. The charging profile of the semi-solid Na–S cell shows four regions similar to those in the discharge profile, suggesting good reversibility of the cell.

We next examine the battery operation when the sulfur loading in its cathode is increased from 1 to 10 and 20 M. Because the sulfur concentration (10 and 20 M) exceeds the solubility of sulfur in tetraglyme at 150 °C (2.3 M), suspended sulfur phase should exist in the suspensions, along with the dissolved sulfur. We find that, when the sulfur concentration in the suspensions increases from 1 to 10 M (see **Figure 4**), the region I still retains the same features as the 1 M case. In this region, the dominant reaction is still the transition from elemental sulfur to dissolved Na_2S_8. As the dissolved elemental sulfur is consumed during discharging, the liquid-phase, suspended sulfur dissolves into the solution to provide reactants and thus contributes to discharging. One typically expects the discharge curve to exhibit a plateau in voltage under such a condition, which is not clearly observed in Figure 4. A possible explanation is that, once the reaction generates the mixture of polysulfides and elemental sulfur, the solubility of sulfur in tetraglyme is greatly increased (e.g., the 1:7 mixture of Na_2S_4 and elemental sulfur can go through reactions to form polysulfides such as Na_2S_5, thus leading to a total sulfur solubility of 55 M in tetraglyme at 150 °C)[9b] and hence the concentration of the elemental sulfur is no longer maintained during discharging. The absence of a voltage plateau is also possibly caused by that the relatively slow solubilization of elemental sulfur compared to the reduction of elemental sulfur, which has been suggested in previous Li–S battery studies.[14b] A key difference between the 1 and 10 M case is the characteristics of region II. Unlike the 1 M case, in which the voltage drops gradually from 2.1 to 1.82 V, the discharge curve for the 10 M case features a short plateau around 2.0 V. While the origins of this plateau are not understood at present, a possible cause is the precipitation of Na_2S_4 during discharging. Because of the high nominal concentration of sulfur in the 10 M case, when all elemental sulfur in the suspension is reduced to S_4^{2-}, the formed Na_2S_4 in the solvent can exceed its solubility (0.19 M as established previously)[9b] and precipitates out of the solution. Similar mechanism has been implicated in previous studies of room-temperature Na–S batteries.[9c,13a] In region III, the discharging behavior of the 1 and 10 M cells are quite similar, suggesting that the underlying electrochemical processes are similar. However, region IV is missing in the 10 M cell. This is most likely caused by the fact that the high sulfur nominal concentration in this cell leads to much more significant precipitation of the reaction product Na_2S_2, which either passivates the active carbon surface or clogs the nanopores in the carbon particles to prevent the further reduction of Na_2S_2 toward Na_2S.

When the sulfur nominal concentration in the cathode suspensions increases further to 20 M, only region I and region II of the discharging curve are retained, and the discharge curve stops at 478 mA h g^{-1}, which is close to the theoretical capacity (418 mA h g^{-1}) of the cell when Na_2S_4 is the final product. This reduction of capacity is likely due to a decrease of the active surface areas by the large amount of Na_2S_4 precipitating out of the solution, which can cause the "sudden death" of the cell.[14a]

In order to understand the interplay of many electrochemical processes during the operation of Na–S batteries, we use numerical simulations to help understand how these processes

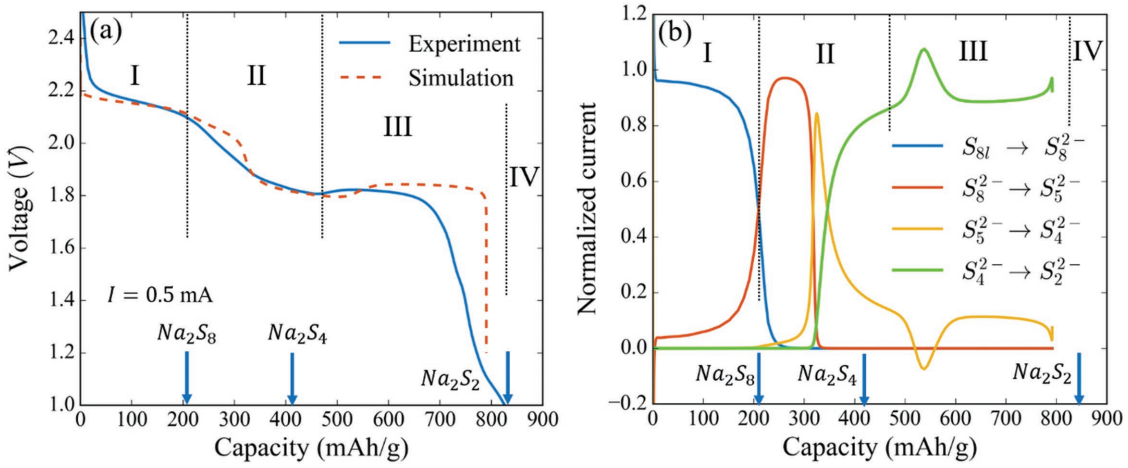

Figure 5. a) Comparison of the discharge curve measured experimentally and computed using 1D model. b) The normalized reaction rate of various electrochemical reactions during discharge obtained from the numerical simulation.

and their interplay affect battery operation. We focus on the discharging behavior of the battery operating in the intermittent flow mode and use a 1D model to describe the physicochemical processes in the battery. Specifically, we adopt the Li–S battery model pioneered by White and his colleagues[14b] and extend it to consider the Na–S battery chemistry. The model considers transport of ions and reactants, electrochemical reactions and precipitation and dissolution of elemental sulfur and polysulfides (see the Supporting Information). Following the common practice in numerical modeling of Li–S and Li–air batteries, battery parameters that can be measured straightforwardly (e.g., sulfur nominal concentration and the conductivity of the membrane) are taken from experimental measurement but other model parameters are adjusted to fit the battery's discharging curve. Solving the battery model using these parameters then provides a detailed view of the reaction, transport, precipitation, and dissolution (if applicable) of all species in the battery. We caution that the model obtained above only gives a qualitative understanding of the key processes in the battery. Nevertheless, prior work in Li–S batteries showed that these simulations can aid the mechanistic understanding of battery operation.[14a,15,16] The above understanding of the electrochemical and other physicochemical processes during the discharge of the proposed intermediate-temperature Na–S battery was incorporated into a 1D model for the proposed Na–S battery (see the Supporting Information for simulation details). Using fitted model parameters, the discharge of Na–S battery cell is solved numerically. **Figure 5**a shows the discharge curves at a sulfur nominal concentration of 1 M (results for the 10 and 20 M cases can be found in the Supporting Information) and the computed and measured discharge curves are in good agreement. Figure 5b shows the current due to various electrochemical reaction in the cathode. The current due to each reaction is normalized by the total discharge current. The normalized currents of each electrochemical reaction shown in Figure 5b further support our previous analysis of the discharging curve. For instance, in region I, the dominant reaction is the transition from dissolved elemental sulfur to S_8^{2-}, which leads to the weak plateau observed in experiment. Furthermore, there are multiple peaks of different reactions appear in region II indicating the gradual degradation of S_8^{2-} to S_n^{2-} ($4 \le n < 8$). At the end of region II, the reaction ($S_4^{2-} \rightarrow S_2^{2-}$) begins to dominant, which implies most polysulfide is in form of Na_2S_4, in agreement with our previous analysis. In region III, the persistent production of Na_2S_2 causes its precipitation (the peak in region III). This liquid–solid phase change leads to the plateau observed in both experiment and numerical analysis. Note that because we did not include reactions leading to the formation of S^{2-} ions and Na_2S_2 in our simulations, the computed discharge curve ends before the appearance of region IV. Neglecting these reactions is reasonable given that their contribution to the total capacity is small and helps reduce the complexity of our model.

The above studies of cell operation under small constant current provide mainly insights into the battery chemistry. We next study the charging and discharging of the Na–S cell under different discharging currents to probe the kinetic aspects of the cell operation. **Figure 6** shows the discharge profiles under different currents for cathode suspensions with 1 and 10 M sulfur nominal concentration. As the discharge current increases, the achievable capacity of the Na–S cell decreases, e.g., for the 1 M case, the cell capacity reduces from 864 mA h g^{-1} at $I = 0.5$ mA ($\approx C/5$) to 350 mA h g^{-1} at $I = 10$ mA. The qualitative features of the discharge curve also change with the increasing current. At $I = 1.0$ mA, the two plateaus observed under $I = 0.5$ mA are still maintained. However, at $I \ge 5$ mA, these two plateaus completely disappear. These behaviors are in qualitative agreement with those observed in Li–S batteries,[17] and the poor performance at elevated current can mainly be attributed to the localized deposition of reaction products (in our case mainly Na_2S_4 and Na_2S_2) over the carbon surfaces. Such localized deposition tends to block some of the active surface areas in the cathode prematurely and thus compromises the effective utilization of the entire cathode.[17] The kinetic behavior of discharge for the 10 M case is similar to that for the 1 M case, but the decrease of the utilizable storage capacity with increasing current is much sharper than the 1 M case. This is expected because the precipitation of reaction products such as Na_2S_4 is more severe when the sulfur nominal concentration in the cathode increases.

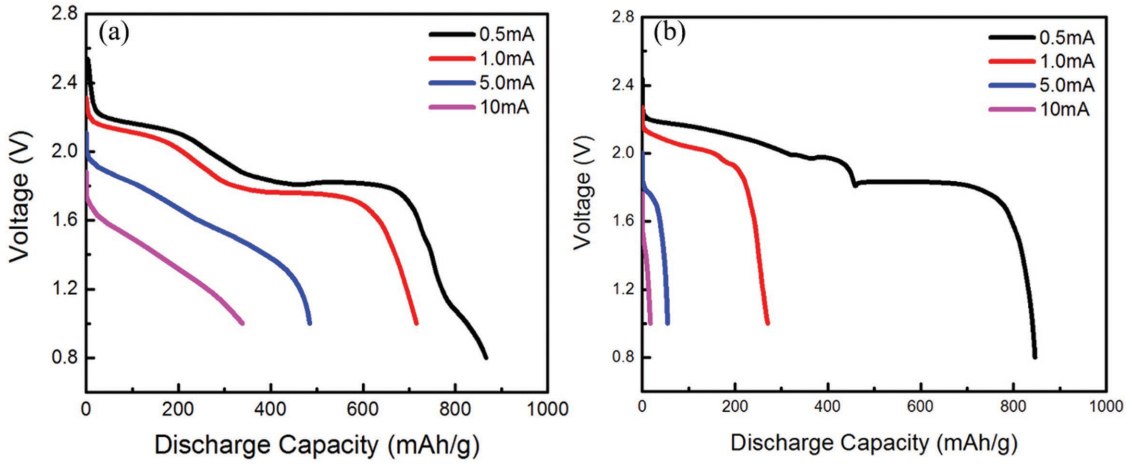

Figure 6. Discharge profiles of semi-solid Na–S battery cells with sulfur nominal concentration of a) 1 M and b) 10 M under various discharging currents. The sulfur suspension catholyte contains 2 vol% Ketjen and the electrolyte is 1 M NaI TEGDME solution. The suspension covered membrane area is around 1.2 cm^2.

Cycling stability of the Na–S cell was also tested using the same static cell design. The sulfur suspension catholyte is composed of 0.5 M sulfur and 2.5 vol% Ketjen in 1 M NaI tetraglyme (TEGDME) solution. Figure S6 shows stable cycling performance of a semi-solid Na–S battery at 150 °C at a constant current of 0.5 mA (≈C/4) between 1 and 2.5 V and the inset figure shows the voltage profile of the 3rd cycle. The initial discharge capacity is around 705 mA h g^{-1} and the capacity retention is around 484 mA h g^{-1} after 55 cycles. The capacity fading mechanism is not clear at this stage and the follow-up investigation is underway.

Having gained insight into the reaction mechanism of semi-solid Na–S cells under static conditions, we next examine its performance under flow conditions. The catholyte in the form of semi-solid suspension has a relative high viscosity and continuous flow mode of catholyte will suffer from large mechanical energy dissipation.[18] Therefore, intermittent flow mode was used for the semi-solid Na–S flow battery tests. The internal flow volume of the power stack is referred to as a unit aliquot of the suspension which is equal to the volume of the gap between the BASE tube and the SS case. **Figure 7** shows the voltage profile and current as a function of time for Na–S flow battery cycling between 1.8 and 2.5 V operated in the intermittent flow mode. The flowable sulfur suspension is composed of 1 M sulfur and 1 vol% Ketjen in 1 M NaI TEGDME solution. The intermittent flow charge–discharge protocol has the following sequence for semi-solid sulfur suspension catholyte: (I) discharging aliquot A which is already replenished the electroactive region of the power stack; (II) pumping the catholyte forward and replacing aliquot A with aliquot B; (III) discharging aliquot B; (IV) charging aliquot B; (V) pumping the catholyte backward and substituting aliquot B with aliquot A; (VI) charging aliquot A. Black solid lines and dashed lines are discharge and charge voltage curves, respectively. Blue line regions

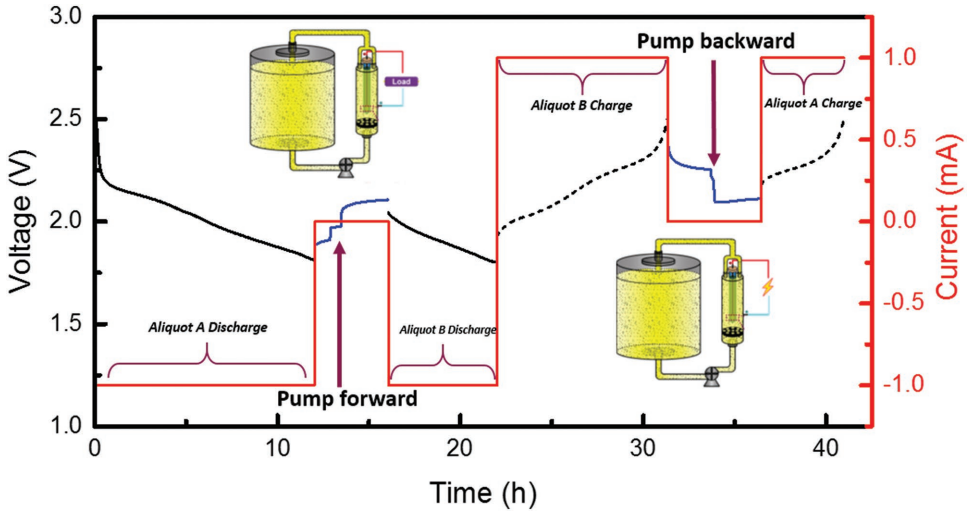

Figure 7. Discharge–charge voltage profiles of three aliquots intermittent flow test cycling between 1.8 and 2.5 V. The sulfur suspension catholyte is composed of 1 M sulfur and 1 vol% Ketjen in 1 M NaI TEGDME solution. The suspension covered membrane area is around 1.2 cm^2. The aliquot A discharge capacity is around 420 mA h g^{-1} sulfur.

indicate the voltage relaxations after each discharge or charge and the onset of the suspension flow. The discharging time for aliquot A is longer than that of aliquot B indicating larger discharge capacity of aliquot A. There are two underlying causes for this phenomenon. The first one is the incomplete replacement of aliquot A with aliquot B during pumping as some of the suspension of aliquot A stays inside the electroactive region of the power stack due to geometrical hindrances (e.g., sharp edges at inlet and outlet). The second one is the charge redistribution by diffusion where charged suspension of aliquot B in the power stack region equilibrates with discharged suspension of aliquot A outside of electroactive zone yet still electrically connected with aliquot B. During step IV of the intermittent flow protocol, the charging time of the aliquot B in the electroactive region is larger than its discharging time as expected due to the charge redistribution with discharged suspension of aliquot A. This interpretation is well aligned with lower charge capacity of aliquot A in step VI. The cutoff voltage for the two-aliquot flow battery test is 1.8 V which is higher than the voltage that leads to the sulfur precipitation region. In order to maximize sulfur utilization, a 1.5 V discharge cutoff voltage is used for the second flow battery test. Figure S3 in the Supporting Information depicts discharge and charge profile of a three aliquots intermittent flow test cycling between 1.5 and 2.5 V. The Columbic efficiency for the two aliquot and three aliquot intermittent flow test are ≈77% and ≈85%, respectively, which will be optimized by better mechanical cell design and precise volume control of the pumping system.

A new semi-solid Na–S flow battery is demonstrated and analyzed. The discharge curve of the battery under static condition shows that two plateau regions at 2.2 and 1.8 V for 1 M sulfur nominal concentration, which corresponds to the consumption of elemental sulfur and the precipitation of Na_2S_2, respectively. Under low discharge currents, storage capacity as high as 864 mA h g^{-1} sulfur, which is much higher than existing Na–S batteries, is demonstrated. Such a high discharge capacity indicates that sulfur is utilized efficiently and discharging proceeds deep into the precipitation of low polysulfides such as Na_2S. Furthermore, the achievable storage capacity decreases as the discharging current increases, and the decrease is more pronounced as the sulfur nominal concentration in the suspension increases. The proposed battery can be highly competitive compared to other grid-scale electrical energy storage system in both performance and cost. In terms of performance, the new battery offers high energy density, efficient utilization of sulfur, and great tolerance of the volume change of electrodes. In terms of cost, the semi-solid flow battery has low materials cost due to the abundance of sodium and sulfur, low manufacturing cost due to the simplified preparation of the catholyte, low operation cost due to the reduced requirement for thermal management of the catholyte storage tank. With further development, the proposed battery may become an attractive solution for future grid-scale energy storage applications.

Supporting Information

Supporting Information is available from the Wiley Online Library or from the author.

Acknowledgements

F.Y., S.M.A.M., T.K.O., and T.Y. contributed equally to this work. This work was funded by the department of mechanical engineering at Virginia Tech. The authors thank Prof. Yet-Ming Chiang and Dr. Liang Su at Massachusetts Institute of Technology for helpful discussions.

Conflict of Interest

The authors declare no conflict of interest.

Keywords

flow batteries, grid energy storage, sodium–sulfur

Received: July 20, 2017
Revised: September 24, 2017
Published online: January 15, 2018

[1] a) B. Dunn, H. Kamath, J. M. Tarascon, *Science* **2011**, *334*, 928; b) H. S. Chen, T. N. Cong, W. Yang, C. Q. Tan, Y. L. Li, Y. L. Ding, *Prog. Nat. Sci.* **2009**, *19*, 291; c) J. Y. Luo, W. J. Cui, P. He, Y. Y. Xia, *Nat. Chem.* **2010**, *2*, 760; d) J. Peters, D. Buchholz, S. Passerini, M. Weil, *Energy Environ. Sci.* **2016**, *9*, 1744. e) R. Xu, J. C. M. Li, J. Lu, K. Amine, I. Belharouak, *J. Mater. Chem. A*, **2015**, *3*, 4170.

[2] a) Z. G. Yang, J. L. Zhang, M. C. W. Kintner-Meyer, X. C. Lu, D. W. Choi, J. P. Lemmon, J. Liu, *Chem. Rev.* **2011**, *111*, 3577; b) W. Wang, Q. T. Luo, B. Li, X. L. Wei, L. Y. Li, Z. G. Yang, *Adv. Funct. Mater.* **2013**, *23*, 970; c) M. Skyllas-Kazacos, M. H. Chakrabarti, S. A. Hajimolana, F. S. Mjalli, M. Saleem, *J. Electrochem. Soc.* **2011**, *158*, R55.

[3] a) M. Duduta, B. Ho, V. C. Wood, P. Limthongkul, V. E. Brunini, W. C. Carter, Y. M. Chiang, *Adv. Energy Mater.* **2011**, *1*, 511; b) S. Hamelet, T. Tzedakis, J. B. Leriche, S. Sailler, D. Larcher, P. L. Taberna, P. Simon, J. M. Tarascona, *J. Electrochem. Soc.* **2012**, *159*, A1360; c) Z. Li, K. C. Smith, Y. J. Dong, N. Baram, F. Y. Fan, J. Xie, P. Limthongkul, W. C. Carter, Y. M. Chiang, *Phys. Chem. Chem. Phys.* **2013**, *15*, 15833; d) F. Y. Fan, W. H. Woodford, Z. Li, N. Baram, K. C. Smith, A. Helal, G. H. McKinley, W. C. Carter, Y. M. Chiang, *Nano Lett.* **2014**, *14*, 2210; e) H. N. Chen, Q. L. Zou, Z. J. Liang, H. Liu, Q. Li, Y. C. Lu, *Nat. Commun.* **2015**, *6*, 5877.

[4] a) Y. Yang, G. Y. Zheng, Y. Cui, *Energy Environ. Sci.* **2013**, *6*, 1552; b) J. F. Li, L. Q. Yang, S. L. Yang, J. Y. Lee, *Adv. Energy Mater.* **2015**, *5*, 24; c) R. Demir-Cakan, M. Morcrette, Gangulibabu, A. Gueguen, R. Dedryvere, J. M. Tarascon, *Energy Environ. Sci.* **2013**, *6*, 176.

[5] a) F. R. Brushett, J. T. Vaughey, A. N. Jansen, *Adv. Energy Mater.* **2012**, *2*, 1390; b) G. Nagarjuna, J. S. Hui, K. J. Cheng, T. Lichtenstein, M. Shen, J. S. Moore, J. Rodriguez-Lopez, *J. Am. Chem. Soc.* **2014**, *136*, 16309; c) T. Janoschka, N. Martin, U. Martin, C. Friebe, S. Morgenstern, H. Hiller, M. D. Hager, U. S. Schubert, *Nature* **2015**, *527*, 78; d) B. Huskinson, M. P. Marshak, C. Suh, S. Er, M. R. Gerhardt, C. J. Galvin, X. D. Chen, A. Aspuru-Guzik, R. G. Gordon, M. J. Aziz, *Nature* **2014**, *505*, 195.

[6] H. D. Pratt, A. J. Rose, C. L. Staiger, D. Ingersoll, T. M. Anderson, *Dalton Trans.* **2011**, *40*, 11396.

[7] Z. H. Lin, A. Firoozabadi, *Fluid Phase Equilib.* **2013**, *360*, 456.

[8] K. B. Hueso, M. Armand, T. Rojo, *Energy Environ. Sci.* **2013**, *6*, 734.

[9] a) P. Adelhelm, P. Hartmann, C. L. Bender, M. Busche, C. Eufinger, J. Janek, *Beilstein J. Nanotechnol.* **2015**, *6*, 1016; b) X. Lu, B. W. Kirby, W. Xu, G. Li, J. Y. Kim, J. P. Lemmon, V. L. Sprenkle, Z. Yang, *Energy*

Environ. Sci. **2013**, *6*, 299; c) H. Ryu, T. Kim, K. Kim, J. H. Ahn, T. Nam, G. Wang, H. J. Ahn, *J. Power Sources* **2011**, *196*, 5186; d) S. Xin, Y. X. Yin, Y. G. Guo, L. J. Wan, *Adv. Mater.* **2014**, *26*, 1261.

[10] G. Weddigen, *J. Electrochem. Soc.* **1980**, *127*, 1225.

[11] a) X. C. Lu, B. W. Kirby, W. Xu, G. S. Li, J. Y. Kim, J. P. Lemmon, V. L. Sprenkle, Z. G. Yang, *Energy Environ. Sci.* **2013**, *6*, 299; b) X. C. Lu, G. S. Li, J. Y. Kim, D. H. Mei, J. P. Lemmon, V. L. Sprenkle, J. Liu, *Nat. Commun.* **2014**, *5*, 4578.

[12] R. M. Darling, K. G. Gallagher, J. A. Kowalski, S. Ha, F. R. Brushett, *Energy Environ. Sci.* **2014**, *7*, 3459.

[13] a) A. Manthiram, X. W. Yu, *Small* **2015**, *11*, 2108; b) I. Kim, J. Y. Park, C. Kim, J. W. Park, J. P. Ahn, J. H. Ahn, K. W. Kim, H. J. Ahn, *J. Electrochem. Soc.* **2016**, *163*, A611.

[14] a) M. Ghaznavi, P. Chen, *J. Power Sources* **2014**, *257*, 402; b) K. Kumaresan, Y. Mikhaylik, R. E. White, *J. Electrochem. Soc.* **2008**, *155*, A576.

[15] a) M. Ghaznavi, P. Chen, *J. Power Sources* **2014**, *257*, 394; b) M. Ghaznavi, P. Chen, *Electrochim. Acta* **2014**, *137*, 575.

[16] V. Thangavel, K. H. Xue, Y. Mammeri, M. Quiroga, A. Mastouri, C. Guery, P. Johansson, M. Morcrette, A. A. Franco, *J. Electrochem. Soc.* **2016**, *163*, A2817.

[17] S. E. Cheon, K. S. Ko, J. H. Cho, S. W. Kim, E. Y. Chin, H. T. Kim, *J. Electrochem. Soc.* **2003**, *150*, A800.

[18] a) V. E. Brunini, Y.-M. Chiang, W. C. Carter, *Electrochim. Acta* **2012**, *69*, 301; b) Z. Li, K. C. Smith, Y. Dong, N. Baram, F. Y. Fan, J. Xie, P. Limthongkul, W. C. Carter, Y.-M. Chiang, *Phys. Chem. Chem. Phys.* **2013**, *15*, 15833.